Stacked volume holographic gratings for extending the operational wavelength range in LED and solar applications

S. Keshri[1], J. Marín-Sáez[2,3], I. Naydenova[1], K. Murphy[1], J. Atencia[3], D. Chemisana[2], S. Garner[4], M.V. Collados[3] and S. Martin[1*]

[1] Centre for Industrial and Engineering Optics, School of Physics and Clinical and Optometric Sciences, College of Science and Health, Technological University Dublin, Ireland
[2] Applied Physics Section of the Environmental Science Department, Polytechnic School, University of Lleida, Jaume II 69, 25001 Lleida, Spain
[3]Applied Physics Department, Aragon Institute of Engineering Research (I3A), Faculty of Science, University of Zaragoza, Pedro Cerbuna 12, 50009 Zaragoza, Spain
[4] Corning Research & Development Corporation, One Riverfront Plaza, Corning, NY 1431, USA
**Corresponding author: suzanne.martin@TUDublin.ie*

Received XX Month XXXX; revised XX Month, XXXX; accepted XX Month XXXX; posted XX Month XXXX (Doc. ID XXXXX); published XX Month XXXX

A novel stacking procedure is presented for Volume Phase Holographic Gratings (VPHGs) recorded in photopolymer material using Corning® Willow® Glass as a flexible substrate, in order to achieve broader angular and spectral selectivity in a diffractive device with high efficiency for solar and LED applications. For the first time, we have shown a device designed for use with a white LED which has the same input and output angles and high efficiency when illuminated by different wavelengths. In this paper, two VPHGs were designed, experimentally recorded and tested when illuminated at normal incidence. The experimental approach is based on stacking two individual gratings in which the spatial frequency and slant have been tailored to the target wavelength and using real-time on-Bragg monitoring of the gratings in order to control the recorded refractive index modulation, thereby optimising each grating efficiency for its design wavelength. Lamination together of the two gratings was enabled by using a flexible glass substrate (Corning® Willow® Glass). Recording conditions were studied in order to minimize the change in diffraction efficiency and peak diffraction angle during lamination and bleaching. The final fabricated stacked device was illuminated by a white light source, and its output spectrally analysed. Compared to a single grating, the stacked device demonstrated a twofold increase in angular and wavelength range. The angular and wavelength selectivity curves are in good agreement with the theoretical prediction for this design. This approach could be used to fabricate stacked lenses for white light LED or solar applications.

http://dx.doi.org/10.1364/AO.99.09999

1. INTRODUCTION

Recently there has been increased interest in VPHGs due to their lightweight, compact nature and high efficiency. VPHGs can be recorded in several materials, but a self-processing photopolymer material is preferred here due to its high diffraction efficiency, linear response, high dynamic range, long shelf lifetime and low cost of production [1]. Much work has been done in the area of single holographic gratings for different applications including spectroscopy [2], data storage [3], solar concentration [4], and lighting [5], but the challenges of angular and wavelength selectivities remain [6]. VPHG typically have high angular and wavelength selectivity, and while that is a beneficial feature for some applications, lower selectivities are desired for others.

In the past few decades, there has been considerable research in the use of diffractive optical elements for LED and solar applications. Since very broad-spectrum white light LEDs have become available, LEDs are increasingly used for everyday lighting applications including automobiles, street lighting and interior lighting. The LED sources themselves are very compact, with dimensions of a few millimetres. However, the highly diverging LED light output means that bulky optics are needed to collimate and re-direct the light in most applications. Reflective and refractive elements are widely available, but they increase the dimensions of the lighting unit by several orders of magnitude and increase the production cost. In lighting applications, the high efficiency of the diffractive lenses is very important, and the change in efficiency due to wavelength can also be significant when a

broadband source is used. A diffractive surface lens on an optical film has been used in the past to control luminosity distribution of LED light [7]; however, surface lenses are not as efficient as volume holographic lenses. Another work involves the splitting of white light LED into its primary colours at three different positions using a reflective volume holographic medium [8]. For LED lighting applications, the optical device should operate in transmission mode and should collimate the beam efficiently. Photopolymer VPHGs, have the potential to replace bulky refractive and reflective elements and allow LEDs to retain their key advantages of a lightweight, small size, flexible format and low cost of production. However, for VPHGs, a key challenge remains; the spectral and angular selectivity of efficient Holographic Optical Elements (HOE) remains high.

HOEs could also be useful in the development of solar light concentrators for use with PhotoVoltaics (PV). HOEs can be used to redirect specific wavelengths toward the PV cell and simply transmit the rest [9] (which may only contribute to its overheating and a possible performance worsening [10]). However, the desired wavelength range is wide, and part of this spectrum is currently lost in the transmitted beam. Stacking of two or more different HOEs, each one designed for a different part of the spectrum, could enhance the spectral range received by the PV cell. As with white light LED, collimation maintaining the same output angle is very important here, so that as much of the light as possible falls on the PV cell. Coupled and stacked holograms have been characterized by Habraken et al. [11] [12]. In other publications, HOEs are stacked with the purpose of increasing the angular range of operation [13], [14] or with the purpose of beam-splitting, so that different parts of the solar spectrum are diffracted towards different PV cells [15], [16]. Two volume gratings have been stacked together in the past to analyse the colour of diffracted light [17]. Stacking multiple elements has also been proposed to correct dispersion for augmented reality applications [18] or to obtain achromatic optical vortices with ultrashort laser pulses [19]. Nevertheless, no studies have been found in the literature on systems with several stacked HOEs having same input and output angle with higher efficiency at two different wavelengths and with the aim of increasing both angular and spectral range of operation.

In this work, the aim is to decrease the angular and wavelength selectivity of the HOE while keeping the input and output angles the same for the designed wavelengths. As mentioned, this has potential applications in the fabrication of holographic lenses for LED lighting and solar concentrators. By producing thinner HOEs, it is possible to have a broader wavelength and angular selectivity; however, the same input-output angle is not possible, as shown in Fig 1(a). One of the solutions is to decrease the angular and wavelength selectivity and keep the same input-output angle by multiplexing two or more gratings in a single thick layer. However, the angular separation between the recorded gratings in multiplexing needs to be significant in order to avoid the recording of unwanted gratings [20], yet small angular and spectral separations are needed to fully cover a broadband source. Also, dynamic range limitations in the material may compromise the efficiency of the individual gratings. For a flexible polymer material, lamination of individual gratings into stacks could be a viable alternative.

Stacked gratings can improve the angular and spectral working range of HOEs, without introducing unwanted additional gratings. If two or more gratings are used, then it is possible to design each one for a different target wavelength range and therefore achieve high efficiency across a broader range of wavelengths. In addition, separate adjustment of the gratings slant and spatial period in each individual grating can allow for the input and output angles to be the same for the two target wavelengths, as shown in the schematic in Fig. 1(b).

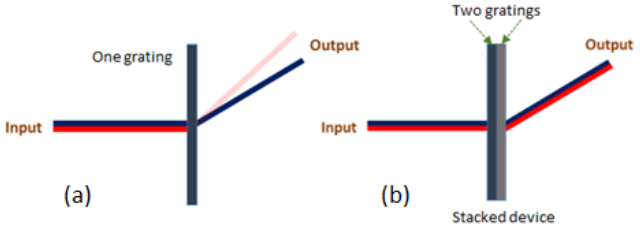

Fig. 1. (a) Diffraction at an individual grating when illuminated by two wavelengths at the same angle. (b) Diffraction at two gratings stacked together, the device is designed to have the same input and output angle for two target wavelengths.

We explore the stacking of photopolymer VPHGs as a means of increasing the working range of HOE devices without introducing crosstalk and spurious gratings. In order to maintain a white light output or to reach a single PV cell, it is critical that the combined device not only functions efficiently at a range of wavelengths but also directs the output light in the same direction for as broad a spectral range as possible. Careful design of each grating for a stacked element is needed in order to achieve this. In this paper, two individual gratings for stacking have been designed and fabricated. In the fabrication of gratings, a glass slide is often used as a substrate for a photopolymer layer. In stacking more than one layer together; the use of thick glass substrates (>1mm) and the index matching between layers is not an optimal solution [21]. This would be highly unsuitable for compact designs and low-cost, mass-produced diffractive optics. Therefore Corning® Willow® Glass is used as a substrate [22], as it has previously been demonstrated as having very high optical quality and sufficient stability for holographic recording [23] [24]. In this work, 100µm thick Corning® Willow® Glass is used as a substrate to record the second grating, with a glass microscope slide as the substrate for the first grating. The designed gratings were fabricated using holographic patterning, using a 532 nm beam as the recording beam and 633 nm and 990 nm beams for real-time on-Bragg monitoring. The results were analyzed for solar and LED applications; with a more detailed study then carried out for target wavelengths for LED applications, including testing with a white light source.

In this paper, in Section 2, the principles of VPHG and the design of the stacked element for solar and LED applications are outlined. In Section 3, the materials and methods used for recording the individual gratings are discussed. The initial

results for the stacked elements are presented in Section 4. In Section 5, a study on the effects influencing the behaviour of the stacked elements is performed, and the final results are presented. Finally, the conclusions are given in Section 6.

2. THEORETICAL BACKGROUND AND DESIGN OF STACKED GRATINGS

A. Theoretical background of volume phase holographic gratings

When two coherent laser beams of the same wavelength interfere inside the volume of a photopolymer material an interference pattern is created which causes polymerization of the monomers. This generates a permanent refractive index modulation inside the volume of the material. Due to this refractive index modulation, a volume phase grating is created, and the orientation of the grating depends on the incidence angle of recording beams with respect to the surface normal of the photosensitive material. When a VPHG is illuminated by the light of any wavelength, a diffracted (first-order) beam will appear in addition to the transmitted (zero-order) beam. The characteristics of the diffracted beam from a VPHG depend, not only on the grating (photonic structure) orientation but also on the angle and wavelength of the incident beam. If two beams of different wavelengths are incident at the same angle on a VPHG, the output efficiency and angle of the diffracted beams will be different (due to dispersion). When a VPHG is illuminated, its diffraction efficiency (η) for a less scattering medium can be defined by Eq.1

$$\eta = \frac{I_{+1}}{I_o + I_{+1}} * 100 \quad \textbf{(1)}$$

where, I_o is the transmission intensity and I_{+1} is the first-order diffracted intensity. The diffracted beam obeys the classical grating equation [25] given by Eq. 2

$$k_i sin\theta_0 + k_d sin\theta_{+1} = \frac{2\pi m}{n\Lambda} \quad \textbf{(2)}$$

where, k_i and k_d are the propagation vector's modulus for the incident and diffracted beams, m=integer (order of diffracted beam, for VPHG m=1), Λ=period of the refractive index modulation (spatial period), θ_0=the angle of incidence in air,θ_{+1}=angle of diffraction in air and n = refractive index of the medium. VPHGs work on the principle of Bragg's law [25], and at the Bragg condition, the angle of incidence equals the angle of diffraction ($\theta_0 = -\theta_{+1}, k_i = k_d = \frac{2\pi}{\lambda}$). Eq. 3 defines the Bragg angle which can be deduced from Eq. 2,

$$\lambda = 2n\Lambda \sin\left(\frac{\theta_{+1} - \theta_0}{2}\right) \quad \textbf{(3)}$$

The maximum efficiency with which light is diffracted by a grating can be approximated using Kogelnik Coupled Wave Theory (KCWT) [26] given in Eq. 4

$$\eta = \left[\frac{Sin(V^2 + E^2)^{1/2}}{(1+\frac{E^2}{V^2})^{1/2}}\right]^2 \quad \textbf{(4)}$$

where modulation parameter V is given by Eq. 5

$$V = \frac{\pi n_1 d}{\lambda\sqrt{cos\alpha_0 cos\alpha_1}} \quad \textbf{(5)}$$

and deviation parameter E is given by Eq. 6 [27]

$$E = \frac{d\vartheta}{2\cos(\theta_{+1})} \quad \textbf{(6)}$$

d= grating thickness, n_1=refractive index modulation, α_0= reference beam angle, α_1=object beam angle and ϑ = dephasing parameter which quantifies the deviation from Bragg condition. From Eq. 4 and Eq. 5, for a layer of given thickness, in order to achieve close to 100% redirection of light of a specific wavelength, Bragg condition must be met (so that E=0) and additionally the magnitude of the refractive index modulation within the material must be carefully controlled and chosen to suit the target wavelength. Higher refractive index modulation is needed to achieve high efficiency for the longer wavelengths.

B. Design of the stacked compound element

Fig. 2 illustrates the design concept for the compound element formed by two stacked VPHGs (G1 and G2). When illuminated with a light source, the two beams are emerging from the first grating, as shown in Fig. 2, are the diffracted beam D_1 (with the efficiency given by Eq. 4) and the transmitted beam T_1 (with the efficiency given by the complement of the diffracted beam's efficiency). These beams enter the second grating (shown here with an exaggerated gap), and each one results in a transmitted and a diffracted beam, whose efficiencies can be determined by applying Eq. 4 again. Therefore, four beams with different directions and efficiencies can be found at the output of the compound element (D_1D_2, D_1T_2, T_1D_2 and T_1T_2). In the proposed design, each grating is designed to efficiently diffract a normally incident beam with a specific target wavelength, λ_1 for G1 and λ_2 for G2. Each grating is not efficient for the other grating's target wavelength so that when illuminating with λ_1 the output beam D_1T_2 will be 100% efficient and when illuminating with λ_2 the output beam T_1D_2 will be 100% efficient. Additionally, the direction of propagation of D_1T_2 with λ_1 and of T_1D_2 with λ_2 must be the same. Wavelengths close to the target ones will be diffracted with directions close to one of the target wavelengths. The direction of D_1D_2 and T_1T_2 will be different but they will have negligible energy.

C. Design of the volume phase holographic gratings for solar and LED applications

In the process of designing stacked elements, two gratings are used for the two target wavelengths; designated G1 and G2 for the LED application and GA and GB for the solar

application. Fig. 3(a) and 3(b) show the target wavelengths (dashed line) on the spectrum of the intended sources.

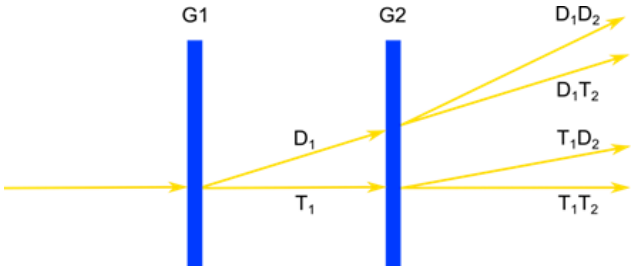

Fig. 2. Schematic of the output beams when illuminating a stacked holographic grating with a wavelength (exaggerated figure).

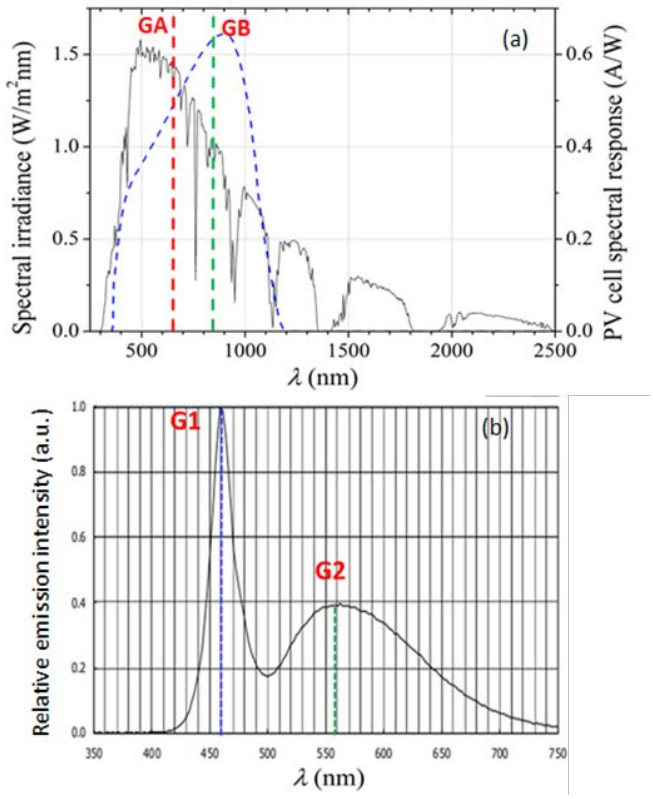

Fig. 3. (a) Absolute irradiance of the sun (black solid curve, left y-axis) and spectral response of a Silicon PV cell (blue dashed curve, right y-axis), with target wavelengths (vertical dashed lines) for gratings (GA & GB) indicated. (b) Relative emission intensity from a typical white LED (Nichia 550D) with target wavelengths (dashed lines) for gratings (G1 & G2) indicated.

When designing each grating, a spatial frequency of the first grating is determined for one of the target wavelengths. The grating is slanted so that incidence at the Bragg angle is designed to be normal incidence. Based on the angle of the diffracted beam from the first grating, the spatial frequency of the second grating is obtained by keeping the output angle equal to that of the first grating and calculating the spatial frequency that will produce same output diffraction angle. Here, the slant angle of the second grating is also changed to ensure the same input-output angle. Diffraction is maximum for incidence along the normal. Next, the required value of the product of the refractive index modulation and the thickness is determined for both gratings to have 100% diffraction efficiency at the target wavelength for which they are designed and perpendicular incidence using equations Eq. 4 and Eq. 5. An optimized photopolymer thickness is chosen such that the compound theoretical wavelength selectivity curves from both gratings cover as much of the spectrum of solar or LED light as possible while reducing crosstalk, thus determining the refractive index modulation. Any grating can be chosen as the first recorded grating as per convenience in the experiment. In this paper, GB is the first recorded grating for solar, and G2 is first recorded grating for LED application. The design parameters were chosen for solar and LED (Nichia 550 D) applications to get equal output beams when illuminated normally and is shown in Table 1. The design parameters here are just one example, and the exact design will vary according to the spectral characteristics of the LED used. Here, the design parameter is those for the Nichia 550D LED.

Due to the complexity of the recording geometry and difficulties in the real-time monitoring of the first-order diffracted beam accurately, it was more convenient to monitor zero-order transmittance, and this has been done throughout the paper. For a thick grating, KCWT predicts only first-order diffraction; therefore, undiffracted light will go into the zero-order and be transmitted. Fig. 4(a) and Fig. 4(b) shows the theoretical zero-order transmittance versus the illuminating wavelength for both gratings with their theoretical compound curves at normal incidence. In each example, the diffraction efficiency is 100% at each of the two target wavelengths (seen as 0% in the zero-order here), with decreasing efficiency moving away from the target (or an increase in the zero-order in this case). The photopolymer layer formulation used in this study is sensitive to green light, so grating recording was carried out at 532 nm. This requires calculation of the appropriate beam angles needed to produce the interference pattern required to obtain the spatial frequencies and slants as outlined in Table 1. $\theta_{1,\,air}$ (°) is the angle between the normal of the material surface and the first (reference) recording beam, in air. $\theta_{2,\,air}$ (°) is the angle between the normal of the material surface and the second (object) beam, in air. The appropriate recording angles for both gratings when recorded at 532 nm are shown in Table 2. During recording, real-time Bragg monitoring (zero-order growth curve) was carried out at an appropriate wavelength to allow accurate stopping of the recording when the desired refractive index modulation was achieved, as this ensured maximum efficiency at the target wavelengths. The chosen probe lasers were 632.8 nm (He-Ne) for G1 and G2 and a 990 nm probe laser for GA and GB. As 632.8 nm and 990 nm are not the target wavelengths, it was necessary to calculate the expected diffraction behaviour of the desired grating at these wavelengths. The angle at which peak efficiency, or minimum value of zero-order transmittance, of the grating, will be observed when illuminated at 632.8 nm and 990 nm. The layer thickness and desired refractive index modulation (from Table 2) are used in Eq. 4 to calculate the target first-order diffraction efficiency expected for the designed gratings when illuminated at 632.8 nm and 990 nm and is shown in Table 3.

Applications	Grating	λ_{target} (nm)	Λ (µm)	SF (l/mm)	Thickness (µm)	n_1	Efficiency (%)	Incidence angle in the air (°)	Diffracted angle in the air (°)	θ_{Slant} (°)
Solar	**GA**	650	1.91	523	150	0.0021	100	0	19.74	6.508
	GB	850	2.50	400	150	0.0028	100	0	19.74	6.507
LED	**G1**	458	2.06	485	150	0.0015	100	0	12.75	4.222
	G2	555	2.50	400	140	0.0019	100	0	12.75	4.231

Table 1: Design parameters for gratings GA & GB for solar and G1 & G2 for LED applications.

Applications	Grating	λ(nm)	$\theta_{1,air}$ (°)	$\theta_{2,air}$ (°)	Target n_1
Solar	**GA**	532	1.78	17.91	0.0021
	GB	532	3.66	15.98	0.0028
LED	**G1**	532	-1.04	13.78	0.0015
	G2	532	0.27	12.48	0.0019

Table 2: Calculated recording parameters for λ=532 nm in order to produce the desired spatial frequency and refractive index modulation, as stated in Table 1.

Applications	Grating	λ_{test} (nm)	η_{+1} (%)	η_0 (%)	θ_{Peak} (º)
Solar	**GA**	990	73	27	-5.15
	GB	990	95	05	-1.62
LED	**G1**	632.8	81.68	18.32	-2.45
	G2	632.8	74	3.92	-0.90

Table 3: Expected Bragg diffraction angles and diffraction efficiencies of gratings designed for solar and LED applications when illuminated by a laser (990 nm for solar and 632.8 nm for LED) (calculated for on-Bragg monitoring during recording).

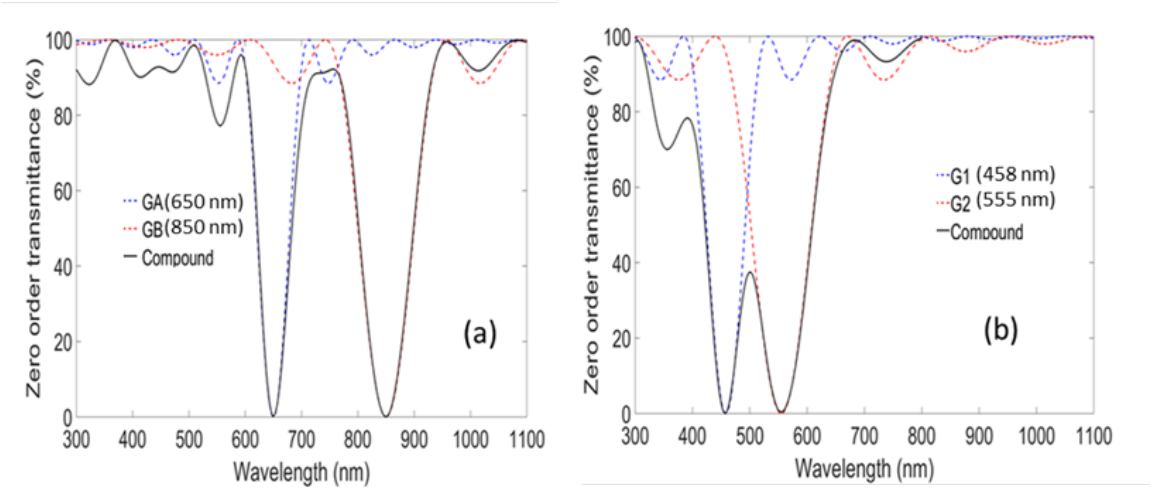

Fig 4. Calculated wavelength selectivity curves of individual gratings and stacked gratings for (a) solar application and (b) LED application when illuminated by white light at normal incidence.

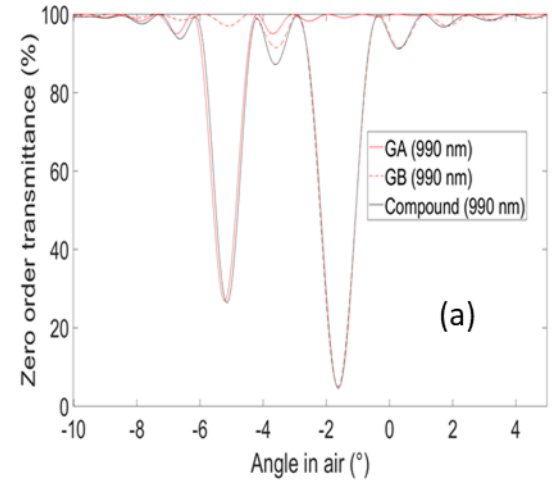

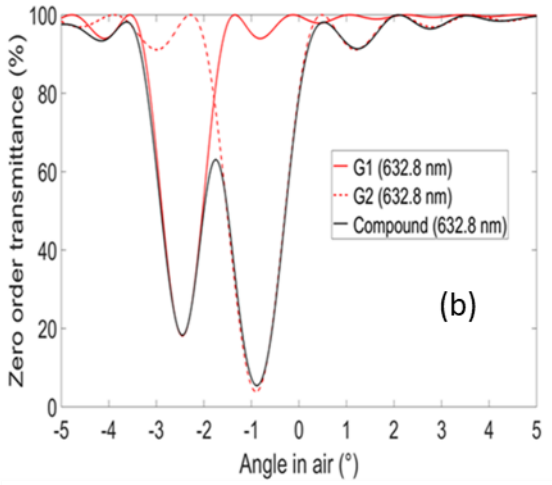

Fig 5. (a) Calculated angular selectivity curves for individual gratings GA, GB and the stacked element for the solar application and (b) G1, G2 and the stacked element for the LED application when illuminated at 632.8 nm.

Since the recorded gratings are probed/tested with a 632.8 nm and 990 nm laser, the zero-order angular selectivity curve at 990 nm (GA, GB, compound) and 632.8 nm (G1, G2, compound) were also calculated. Fig. 5(a) and Fig. 5(b) are the theoretical zero-order transmittance versus the angle of illumination in the air for each individual grating, together with the compound curve. G1, for example, is designed to have 100% efficiency for a 458 nm beam (line 3 table 1) which equates to a maximum diffraction efficiency of ≈82% (18% for zero-order) when probed by He-Ne laser (Line 3, table 3). When the zero-order angular selectivity curve is plotted (Fig. 5(b)), this equates to a trough that reaches 18 % (Line 3 table 3, and figure 5). In the next section, the material used for recording and experimental procedure has been described.

3. MATERIALS AND EXPERIMENTAL METHODS

A. Flexible glass substrate

As mentioned previously, the assembly of a multi-layer stacked VPHG relies on the use of a flexible glass substrate. This is primarily due to the combined mechanical and optical attributes of flexible glass compared to alternative substrate materials. The specific flexible glass used in this study is 100 µm thick Corning® Willow® Glass. The general properties of flexible glass have been previously described [23] [24]. The most significant mechanical properties relevant to stacked VPHG applications include, the Willow Glass having a Youngs Modulus in the range of 73 GPa, this results in a reduced rigidity that enables roller-based lamination and solution coating processes. In the overall VPHG design optimization, vacuum deposition processes can be used to deposit anti-reflection or index-matching layers. Additionally, the Willow Glass substrate has a surface roughness (Ra) < 0.5 nm, which enables smooth interfaces with the photopolymer layers. In terms of optical properties, Fig. 6(a) shows the optical transmission of both flexible 100 µm and rigid 630 µm glass substrates of similar compositions. Additionally, the flexible glass is isotropic with the refractive index shown in Fig. 6(b). Use of flexible 100 µm thick glass in stacked VPHG designs, enables an overall structure much more dimensionally compact (and with lower parallax) than can be achieved using rigid glass and with higher optical efficiency than achievable with representative polymer films.

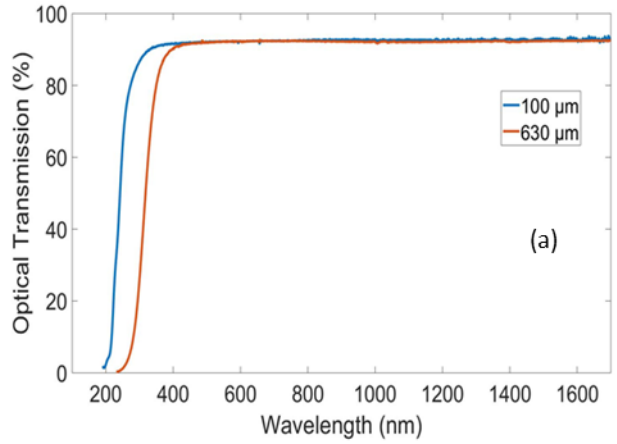

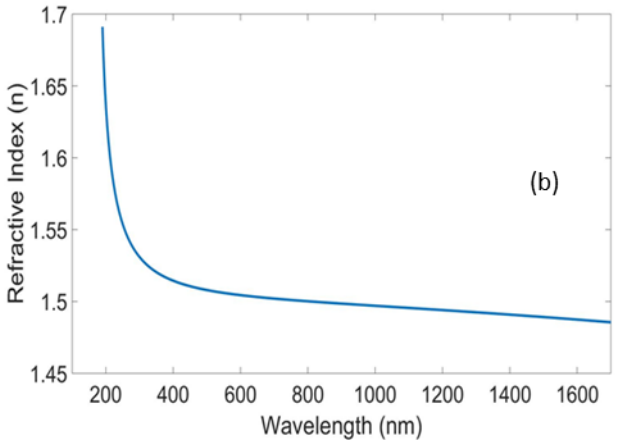

Fig. 6. (a) Optical transmission of Willow Glass and a rigid glass of similar composition. (b) Refractive index of Willow Glass.

B. Photopolymer characteristics

In this paper, photopolymer has been used as the photosensitive holographic recording material. In the

preparation of the photopolymer solution, 100 ml deionized water was mixed with 10g polyvinyl alcohol (PVA). After complete dissolution of PVA in water, the solution was mixed with 0.6g or 0.8g of acrylamide (0.6g for LED and 0.8g for solar application, since for longer wavelength higher index modulation is needed to achieve higher efficiency), 0.2g N-N methylene bis-acrylamide, 2ml triethanolamine and 4ml of erythrosine B [21]. The solution is then stirred until it is completely dissolved. A photopolymer layer is prepared by putting the solution on a standard glass microscope slide (1 mm thick) and on a flexible Willow Glass substrate and kept in the darkroom for two-three days until it is dry. The layers are prepared by deposition of a fixed volume on a known substrate area supported by a levelled marble surface, using a pipette. All layer thicknesses quoted are for the final dry layer thickness. In the experiment, the photopolymer layer having glass slide as a substrate is recorded first. The complete procedure of recording and stacking is shown in the next section. The average refractive index of the photopolymer layer is 1.5. The photopolymer is self-developing material and does not require post-treatment other than bleaching by light exposure.

C. Stacking procedure and experimental setup

In the experimental work, first, a grating whose substrate is a standard glass microscope slide is recorded and exposed to normal daylight for two days. A fresh photopolymer layer is then coated onto a flexible substrate, Willow Glass (100 µm thick) and left in a dark room until dry. After drying, the fresh photopolymer layer was laminated on top of the first recorded grating in such a manner that two photopolymer layers face one another. A second grating is then recorded in the fresh photopolymer layer and the stacked element left to bleach in normal daylight. The method of first laminating photopolymer layer and recording the second grating is done to minimize any changes in the dimension of the second grating. In the stacked element, the structural edges of first and second gratings coincide together. The layer arrangement of compound elements follows glass-photopolymer-photopolymer-flexible glass. Fig. 7 presents the step-by-step stacking procedure.

The experimental setup used to record the gratings is shown in Fig. 8. A green laser (532 nm, Ventus 532, Laser Quantum) passes through a spatial filter, collimator lens, aperture and is then divided into two optical paths (reference and object beam) by a non-polarizing beam splitter. The reference and object beam interfere inside the volume of the photosensitive material, and an interference pattern is formed. The intensity of the reference beam and object beam is equalized before recording, and the angles of these recording beams were adjusted to match the theoretical calculation shown in Table 2. The diameter of reference and object beams were 14 mm, hence the recording area on the photopolymer layer was 150 mm^2. A He-Ne (632.8 nm) laser has been used for real-time Bragg monitoring of G1 and G2, while a 990 nm IR laser has been used for real-time monitoring of GA and GB.

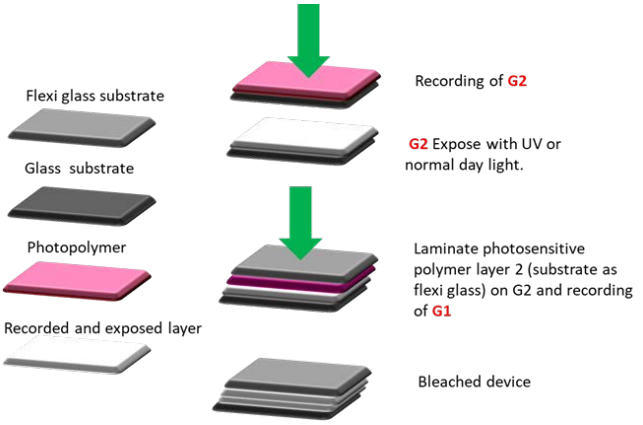

Fig. 7. Recording and stacking procedure.

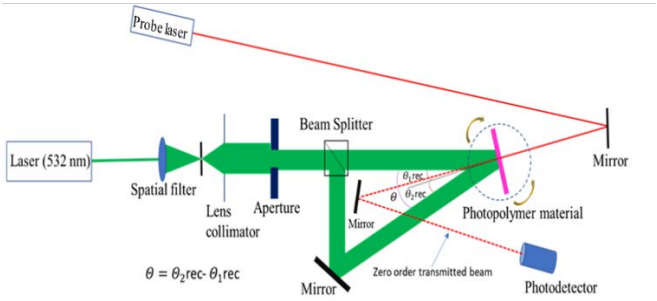

Fig. 8. Experimental set-up for the recording and real-time monitoring of the individual gratings for stacking.

Due to the complexity of the recording geometry and difficulties in the monitoring of the first-order diffracted beam accurately, it was more convenient to monitor zero-order transmittance, and this has been done throughout the paper. As the operation regime of the grating is thick, according to KCWT, the first-order diffraction efficiency can be approximated as the light which is not going into the zero-order transmittance. After each recording, in order to get data on the gratings and to measure index modulation, the recorded gratings were illuminated by the same He-Ne or 990 nm laser over a wide range of angles to obtain a zero-order angular selectivity curve. In all zero-order angular selectivity curves shown here, 0° is defined as normal incidence, perpendicular to the plane of the element and the angle shown is the angular deviation in air. The sequence of grating recording was not itself important, but it was necessary to ensure that for the second recording, the recording beams reached the unexposed photopolymer layer first so as not to be disturbed by the existing grating.

4. RESULTS AND ANALYSIS

A. Results and analysis for LED and solar applications

Using the above experimental procedure, two gratings were recorded with a total recording intensity of 0.85 mW/cm^2 at recording angles appropriate for the LED application. The first recorded grating was G2 and the second recorded grating was G1. G2 was recorded using the recording parameters from Table 2, and its zero-order growth curve is shown in Fig. 9(a). Theoretical and experimental zero-order

angular selectivity curves (before bleaching of G2) are shown in Fig 9(b). The zero-order growth curve of the second recorded grating G1 is plotted in Fig 9(c). Theoretical and experimental zero-order angular selectivity curve of the stacked element (compound element) before bleaching is presented in Fig. 9(d). In the growth curves, the optical losses have been corrected by capturing the transmittance at Bragg angle and in the angular selectivity curve, the reflection losses are negligible as the range of incidence angle is very small.

For G2, the good agreement between the final value observed in the zero-order growth curve of Fig. 9(a) when the recording was stopped, and the minimum experimental value (corresponding to maximum diffraction) observed in Fig. 9(b) shows that the grating growth was accurately monitored at the Bragg angle during recording. Its agreement with the minimum value on the theoretical curve shows that the grating growth was stopped at the appropriate point, and the refractive index modulation of the grating should now be close to the desired value. The fit between experimental and theoretical curves is also very good in terms of angular position, indicating that the slant and spatial frequency are very close to the design value. It should be noted that the experimental curve is a little broader than the theoretical curve, which may be due to small variation in thickness of photopolymer medium. Similarly, the final transmittance value for G1 in Fig. 9(c) and the experimental minimum transmittance value (for G1) observed in Fig. 9(d) differ by only 1-2%, indicating accurate on-Bragg monitoring for the growth of G1. The difference between the experimental on-Bragg diffraction efficiency and the theoretical on-Bragg diffraction efficiency here is also around 1-2% which indicates a small but tolerable deviation from the target refractive index modulation for G1. The angular position of G1 is only mismatched by ≈ 0.1°. However, the previously well-matched G2 grating has now dropped more than 4-5% in efficiency and shifted its angular position by approximately 0.5°. This indicates that the first grating was altered during the process of adding the second grating.

Similar changes were observed in all samples recorded for solar applications. The experimental result for stacked gratings designed for solar application is shown in Fig. 10. Fig.10(a) shows the real-time zero-order growth curve for grating GB, obtained using a 990 nm probe beam. Fig. 10(b) presents the experimental and theoretical zero-order Bragg selectivity curve obtained using the same probe beam. A good match is observed between the experimental data and the theoretical curve, confirming the successful recording of GB. Fig. 10(c) presents the real-time zero-order growth curve for the recording of GA, obtained by probing during recording using a 990 nm probe beam. Fig 10(d) then shows the experimental and theoretical zero-order Bragg selectivity curve for the bleached stacked device. Here efficiency of the first-recorded grating, GB, is reduced by 4-5% after the second grating was added, as observed above. In this example, bleaching has significantly reduced the efficiency of GA. There is also a 0.5° difference between the angle at which maximum diffraction occurs in the theoretical and experimental curves.

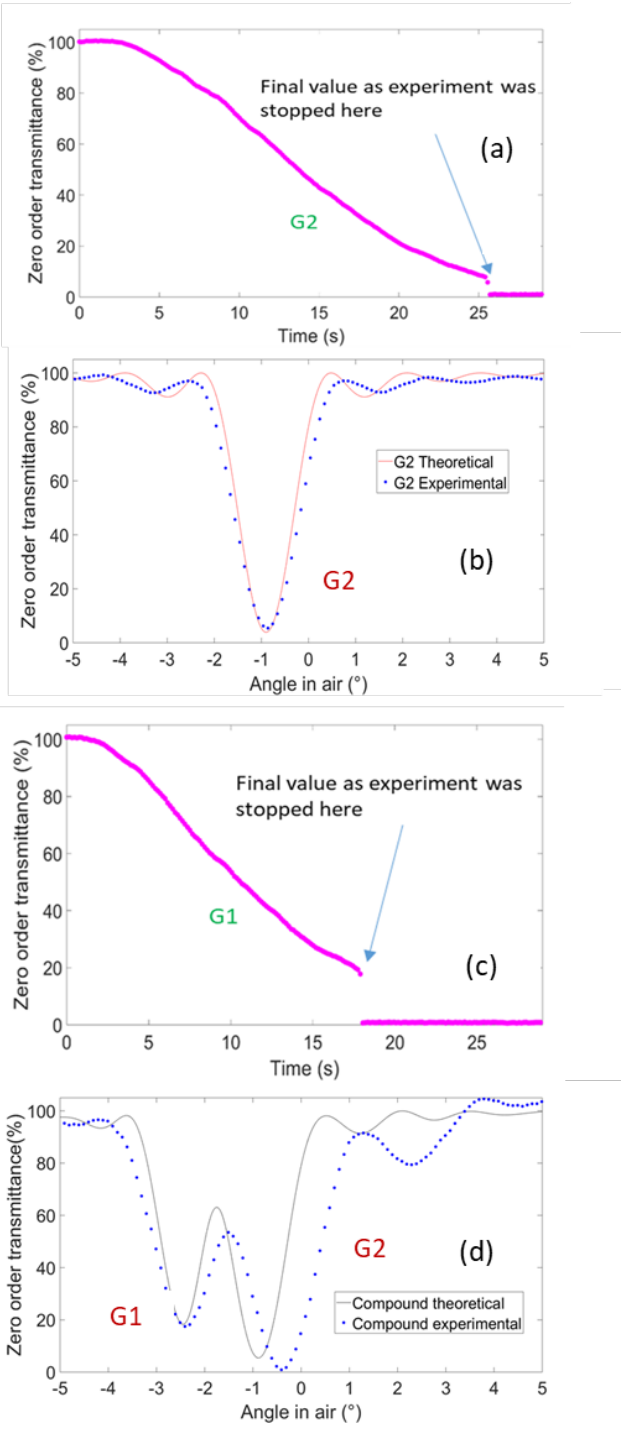

Fig. 9. (a) The zero-order growth curve obtained during the recording of G2 . (b) Angular selectivity curve for the recorded grating G2 (c) The zero-order growth curve for the recording of G1. (d) Angular selectivity curve for the stacked gratings (G2 & G1). The illumination wavelength is 632.8 nm for all four graphs.

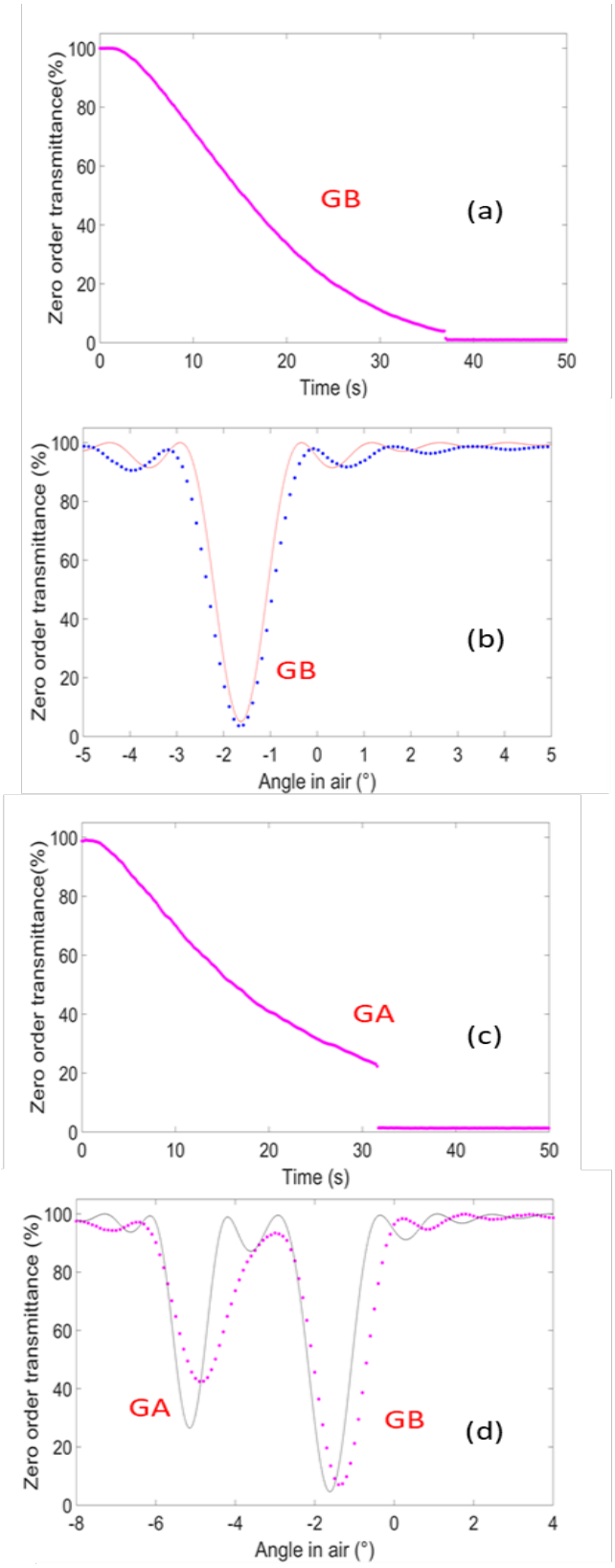

Fig. 10. (a) The zero-order growth curve obtained during the recording of GB. (b) Angular selectivity curve when for GB (c) The zero-order growth curve for GA. (d) Angular selectivity curve for stacked gratings (GB & GA). The illumination wavelength is 990 nm for all four graphs.

Some of the potential reasons for the changes observed in the efficiency and angular position are examined in the next section using the gratings designed for LED applications as an example, and an improved recording protocol is explored.

5. STUDY OF THE INFLUENCE OF LAMINATION AND BLEACHING ON THE GRATING BEHAVIOUR

A. Effect of lamination on a volume grating

Lamination pressure was examined to investigate its effect on the photonic structure of the gratings. A set of four gratings were recorded at a spatial frequency of 1000 l/mm and a slant angle of 15°. Large slant angles and a high spatial frequency were chosen so that the effect of pressure on the grating would be greater and more easily observed. These gratings were then subjected to typical pressure used for laminating a flexible glass onto the gratings. The gratings were illuminated over a wide range of angles by a He-Ne laser before and after the applied pressure. It was observed that the angular position of minimum value shifted by a consistent 0.8° ± 0.05 for these 4 samples, as shown in Fig. 11.

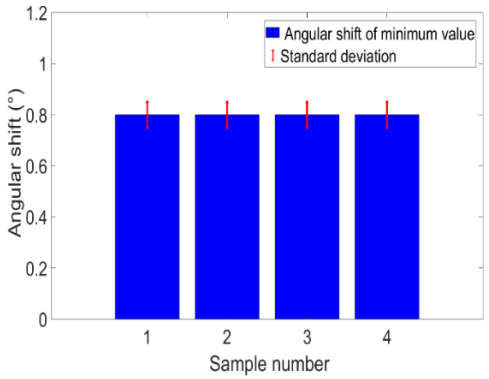

Fig. 11. Change in the angular position of minimum value after lamination in four different samples with error bars showing the standard deviation.

A shift of 0.8° in the diffracted beam for a 1000 lines/mm grating recorded with a 15° slant implies 0.4° change of slant angle which corresponds to a 2.8% change in the layer thickness [28]. Based on the above, angular detuning of up to 0.4° could be expected in the designed gratings (considering slant of 6-7°) as they are laminated [28]. Small changes in diffraction efficiency were also noted (average 5%), but neither the magnitude nor the direction of the change was consistent across these samples.

B. A bleaching effect on G2

Generally speaking, after the fabrication of a photopolymer material device, further daylight on a device will not cause the diffraction efficiency to change significantly as most of the monomer has polymerized and any remaining monomer conversion happens in a uniform manner across the grating. Yet significant changes have been observed in these experiments.

Analysis of the bleaching effect on these photopolymer devices is important because careful control of the refractive index modulation is critical to the grating performance, in these applications. From Fig. 9(d) and 10(d), we observed that after the addition of a second grating, the efficiency of the first grating (GB for Solar and G2 for LED) is reduced. Here, the effect of bleaching is studied in detail for grating G2 since it was the first grating for LED application. G2 gratings were recorded in five photopolymer layers with glass microscope slides as their substrate with same recording conditions as used above (total intensity=0.85 mW/cm^2), and all were bleached in normal daylight for two days. Zero-order angular selectivity curves were obtained by probing the gratings at 632.8 nm for a wide range of incidence angles before and after bleaching. Fig. 12 shows the first-order peak efficiency for five samples with its standard deviation before and after bleaching at two different recording intensity. It was found that there was a significant drop in the peak efficiency (increase in the minimum value of the zero-order curve) of G2 by 15-20% after bleaching in all five gratings when they were recorded with 0.85 mW/cm^2. This drop is likely to be due to the polymerization of the remaining monomer, which would alter the refractive index modulation slightly. Usually, thinner layers are used and thus, devices are exposed almost to saturation level in the holographic patterning step. Here, however, in order to tightly control the refractive index modulation, the recording is stopped 'early' (before saturation occurs) and a larger-than-usual amount of unpolymerized monomer remains. In order to increase the stability of the gratings and to reach a saturation level, five G2 gratings were also recorded in a higher intensity regime (total intensity =1.45 mW/cm^2) and the measurements repeated. It should be noted that the exposure energy in the low and high-intensity recordings was not the same as the aim was to reach the required index modulation.

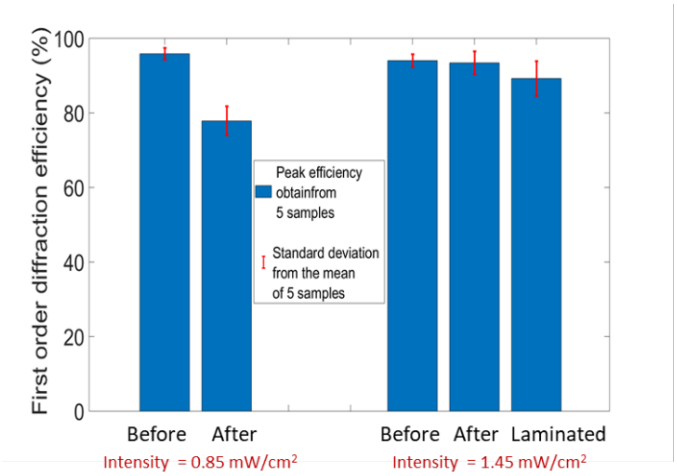

Fig. 12. Effect of daylight bleaching on the diffraction efficiency of grating G2 when recorded with lower (0.85 mW/cm^2) and higher (1.45 mW/cm^2) intensities. The effects of lamination for gratings recorded with 1.45 mW/cm^2 intensity are also shown.

From Fig. 12, It can be concluded that the high-intensity recording condition causes less change in efficiency after bleaching. The effect of lamination was only studied for the samples recorded with the higher intensity since at high efficiency change in efficiency was less. For the considered grating designs, it can be concluded that lamination of a photopolymer layer was accompanied by a small drop in efficiency and a shift in minimum value/peak efficiency angular position. Bleaching causes the greatest changes in the diffraction efficiency, but this can be improved by recording with a higher intensity.

B. Demonstration of a stacked element

A final grating G2 was recorded at higher intensities (1.45 mW/cm^2) as discussed in the previous subsection. After recording, G2 was bleached, and a photopolymer layer was laminated onto it and G1 was recorded with the same intensity. The theoretical and experimental zero-order angular selectivity curves of the completely bleached stacked (compound) gratings are shown in Fig. 13(a). Fig. 13(a) demonstrate a wider zero-order angular selectivity curve which is designed to be suitable for a white LED (parameters detailed in table 3). Comparing these curves, it can be seen there is a good match in the efficiency of G2, while there is still a mismatch of around 7-9% in the efficiency of G1, despite the higher intensity recording. However, the angular position of the minimum value of G2 and G1 match the theoretical position to within ± 0.5°.

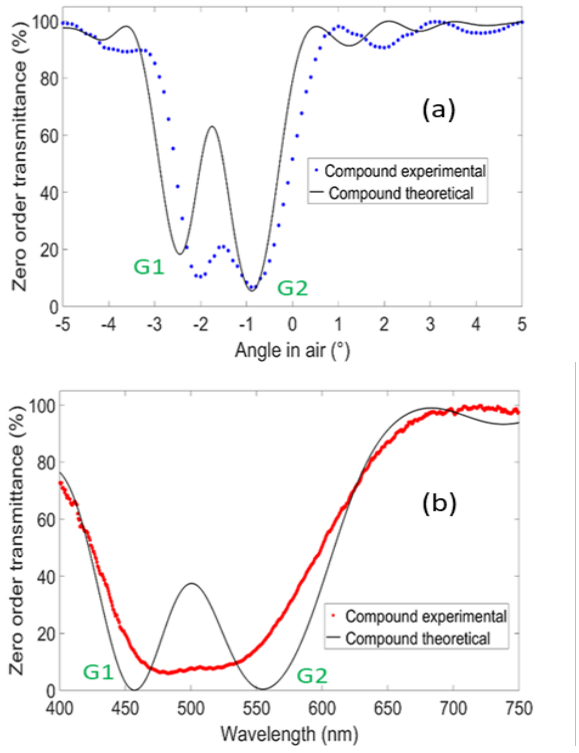

Fig. 13. (a) Zero-order angular selectivity curve when stacked gratings (G1 & G2) were illuminated by He-Ne laser. (b) Experimental wavelength selectivity of the stacked gratings when illuminated by white light source perpendicularly (Theoretical G1 and G2 wavelength included).

Fig. 13(b) shows the theoretical and experimental zero-order wavelength selectivity curves for the compound element when a white light source (AvaLight-HAL) illuminates the

stacked device at normal incidence. Compared to a single grating, the experimental results of the stacked device show a broader wavelength selectivity curve, with no significant crosstalk gratings, and covering the wavelength region of the LED (Nichia 550D). Fig. 13(b) experimental curve cover at least 50 % efficiency for the wavelength range 425-600 nm.

The experimental curve is a reasonably approximate match for the theoretical curve, and it may be possible to further improve on the deviations in diffraction efficiency and angular position by addressing issues of bleaching, lamination and crosstalk in more depth. These laminated devices display potential for broadening the angular and spectral range of DOEs for LED and solar applications. However, it must be borne in mind that further work is needed to precisely reproduce the theoretical design, both in terms of high efficiency and accurate re-direction of the light by the photonic structure.

6. CONCLUSION

A novel procedure for stacking two VPHGs has been proposed and experimentally tested with the aim of making a diffractive device with a broader angular and spectral working range. The device is designed to (1) have the same input-output angle for two different target wavelengths and (2) have a diffraction efficiency that approaches 100% for the target wavelength. Gratings for wavelengths appropriate for solar and LED applications were designed and tested. Successful control of the refractive index modulation growth during grating recording was achieved in order to reach the target efficiencies and control of the recording angles was confirmed to successfully record appropriate grating structures; however, Bragg analysis showed that the bleaching and lamination processes had introduced small changes in the refractive index modulation and angular position of the peak efficiency (diffraction angle).

A higher recording intensity improved the stability of the photonic structure, and the refined process was successfully demonstrated here for a stacked element designed for two key wavelengths in a white LED for the first time. A broad spectral range (425-600 nm) was experimentally demonstrated for this stacked device which matched well with the predicted theoretical wavelength selectivity of the combined gratings and was approximately double the spectral range for a single grating. This approach shows promise for the production of laminated stacked elements (more than two VPHGs also) for use in broad-spectrum applications, although further work is needed to improve the control over the lamination pressure applied.

Funding. Technological University Dublin (Fiosraigh Dean of Graduate Students Award); Enterprise Ireland (CF20144622); Diputación General de Aragón-Fondo Social Europeo (TOL research group, E44_17R). Ministerio de Economía y Competitividad (ENE2016-81040-R). Generalitat de Catalunya (2017FI_B2_00127). Universitat de Lleida.

Acknowledgement.

The authors wish to thank the FOCAS Research Institute.

References

1. D. Jurbergs, F.K. Bruder, F. Deuber, T. Fäcke, R. Hagen, D. Hönel, T. Rölle, M.-S. Weiser, and A. Volkov, "New recording materials for the holographic industry," **7233**, 72330K (2009).
2. S.C. Barden,J.A Arns.,W.S. Colburn. Volume-phase holographic gratings and their potential for astronomical applications. *Soc Photo-Optical Instrum Eng Conf Ser*. 1998; 3355(March):866-876. doi:10.1117/12.316806
3. D. Bade,I. Naydenova, V. Toal, S. Martin, "Recording of high efficiency volume Bragg gratings in a photopolymer using diffraction from very weak pre-recorded gratings", *Opt Data Process Storage*. 2016;2(1):7-14. doi:10.1515/odps-2016-0002
4. J. Marín-Sáez, J. Atencia, D. Chemisana, and M.-V. Collados, "Characterization of volume holographic optical elements recorded in Bayfol HX photopolymer for solar photovoltaic applications," Opt. Express **24**, A720-730 (2016).
5. S. Keshri, K. Murphy, V. Toal, I. Naydenova, S. Martin,"Development of a photopolymer holographic lens for collimation of light from a green light-emitting diode". *Appl Opt*. 2018; 57(22): E163. doi:10.1364/AO.57.00E163
6. I. Naydenova *et al.*, "Photopolymer Holographic Optical Elements for Application in Solar Energy Concentrators," *Hologr. - Basic Princ. Contemp. Appl.*, 2013.
7. A. Motogaito and K. Hiramatsu, "Fabrication of Binary Diffractive Lenses and the Application to LED Lighting for Controlling Luminosity Distribution," *Opt. Photonics J.*, vol. 3, no. March, pp. 67–73, 2013.RGB –VLC
8. Z. Shen, T. Lan, L. Wang, and G. Ni, "Colour demultiplexer using angularly multiplexed volume holograms as a receiver optical end for VLC based on RGB white LED," *Opt. Commun.*, vol. 333, pp. 139–145, 2014.
9. M. V. Collados, D. Chemisana, and J. Atencia, "Holographic solar energy systems: The role of optical elements," Renew. Sustain. Energy Rev. 59, 130–140 (2016)
10. E. Radziemska, "Thermal performance of Si and GaAs based solar cells and modules: a review," Prog. Energy Combust. Sci. 29, 407–424 (2003).
11. N. Servagent, S. Habraken et al.: Coupled holograms, 13th European Symposium on Optoelectronics, Paris (France), ESI Publications, Paris (1993), pp. 578-583
12. S. Habraken et al.: Characterisation of stacked reflection holograms, 14th European Symposium on Optoelectronics, Paris (France), ESI Publications, Paris (1995), pp. 452-458).
13. D. Zhang, J. Castro,R. Kostuk, "One-axis tracking holographic planar concentrator systems", Journal of Photonics for Energy, 1 (2011), http://doi.org/ 10.1117/1.3590943

14. S. Martin, H. Akbari,S. Keshri, D. Bade,I. Naydenova, K. Murphy, V. Toal, “Holographically Recorded Low Spatial Frequency Volume Bragg Gratings and Holographic Optical Elements”, Holographic Materials and Optical Systems, InTech 2017, https://doi.org/ 10.5772/67296

15. K. Froehlich, E. Wagemann,H. Schulat, H. Schuette, C. Stojanoff, “Fabrication and test of a holographic concentrator for two-colour PV operation” Proceedings of SPIE, 2255 (1994), https://doi.org/10.1117/12.185419]

16. Y. Wu, B. Chrysler, R. Kostuk, “Design and fabrication of cascaded dichromate gelatin holographic filters for spectrum-splitting PV systems”, Journal of Photonics for Energy, 8 (2018), https://doi.org/10.1117/1.JPE.8.017001]).

17. H.D Tholl, R. Kubiza, C.G. Christo, “Stacked volume holograms as light directing elements”, Optical Materials Technology for Energy Efficiency and Solar Energy Conversion XIII, vol 2255 ,1994

18. H. Chen, Y. Weng, D. Xu, N. V Tabiryan, and S. Wu, “Beam steering for virtual / augmented reality displays with a cycloidal diffractive waveplate,” vol. 24, no. 7, pp. 2287–2289, 2016.

19. J. Atencia, M.V. Collados, M. Quintanilla, J. Marín-Sáez, I.J. Sola, “Holographic optical element to generate achromatic vortices”, Optics Express 2013, 21(18), 21056-21061, doi:10.1364/OE.21.021056

20. L. Cui, H. Gao, P. Dong, J. Zhou, D. Liu, “Diffraction from angular multiplexing slanted volume hologram gratings,” vol. 116, pp. 118–122, 2005.

21. H. Akbari,I. Naydenova,S. Martin. “Using Acrylamide Based Photopolymers for Fabrication of Holographic Optical Elements in Solar Energy Applications”. *Appl Opt 53*. 2014:1343-1353. doi:10.1364/AO.53.001343

22. H. Akbari,I. Naydenova,L. Persechini ,S.M. Garner,P. Cimo ,S. Martin. “Diffractive optical elements with a large angle of operation recorded in acrylamide-based photopolymer on flexible substrates”. *Int J Polym Sci*. 2014; 2014. doi:10.1155/2014/918285

23. S. Garner, S. Glaesemann, X. Li, “Ultra-slim flexible glass for roll-to-roll electronic device fabrication,” *Appl. Phys. A*, v.116, pp.403-407, 2014.

24. S.M. Garner, (Ed.). (2017) *Flexible Glass: Enabling Thin, Lightweight, and Flexible Electronics*. Hoboken, NJ: Wiley-Scrivener.

25. G.E.M Jauncey, "The scattering of x-rays and Bragg’s law” Proc.Natl. Acad .Sci. USA **10**, 57-60(1924).

26. H. Kogelnik, "Coupled wave theory for thick hologram gratings,” The Bell System Technical Journal 48(9), 2909-2947 (1969).

27. R. Syms, Practical Volume Holography (Oxford University Press), 1990

28. M. Moothanchery, I. Naydenova, and V.Toal, “Studies of shrinkage as a result of holographic recording in acrylamide based photopolymer film”, Appl. Physics, A.104, 899-902, May 2011